Talanta 225 (2021) 122072

Contents lists available at ScienceDirect

Talanta

journal homepage: www.elsevier.com/locate/talanta

In-situ anchoring bimetallic nanoparticles on covalent organic framework as an ultrasensitive electrochemical sensor for levodopa detection

Xin Sun [a,1], Na Wang [b,1], Yao Xie [a], Huacong Chu [a], Yang Wang [a,*], Yi Wang [c,**]

[a] School of Chemistry and Chemical Engineering, Yangzhou University, Yangzhou, 225002, PR China
[b] Key Laboratory of Systems Biomedicine (Ministry of Education) and Collaborative Innovation Center of Systems Biomedicine, Shanghai Jiao Tong University, 200240, China
[c] School of Biomedical Engineering, School of Ophthalmology & Optometry, Wenzhou Medical University, Wenzhou, 325027, China

ARTICLE INFO

Keywords:
TAPB-DMTP-COF
Bimetallic nanoparticles
Electrochemical sensor
Levodopa detection

ABSTRACT

Covalent organic frameworks (COFs) have been studied in many fields. However, their electrochemical properties were seldom reported. In this work, a novel high electrocatalytic material was synthesized by incorporating bimetallic nanoparticles (AgCoNPs) in a two-dimensional (2D) porous TAPB-DMTP-COF, (AgCo/TAPB-DMTP-COF, TAPB, 1,3,5-tris(4-aminophenyl)benzene; DMTP, 2,5-dimethoxyterephaldehyde). Subsequently, the resulting composite was further used to construct a novel electrochemical sensor for the ultrasensitive determination of levodopa. The analytical performance has been improved significantly due to the synergistic effect of both TAPB-DMTP-COF and AgCoNPs by increasing effective electroactive surface area and electron transfer efficiency. The linear detection range of the levodopa sensor was 0.010–100 μmol L^{-1}. The limits of detection and quantitation were found to be 0.002 and 0.006 μmol L^{-1}, respectively. Moreover, the sensor exhibits an excellent stability and maintains its catalytic activity after 100 scanning rounds. The applicability of the electrochemical sensor was successfully applied for the determination of levodopa content in human urine and blood serum samples. Our study not only supplies a useful tool to accurately detect levodopa in actual samples and, meanwhile, but paves a feasible way to unlock high performance 2D COF based electrode materials.

1. Introduction

Parkinson's disease is a neurodegenerative disease caused from a lack of dopamine in the brain [1]. This pathological state will lead static tremor, postural difficulties, rigidity and loss of balance, which could profoundly impact the patient's life quality [2]. As an essential predecessor of dopamine, levodopa is one of the most effective therapeutic drugs for parkinson's disease, because it can cross the blood-brain barrier and transform into dopamine [3,4]. However, in excess of levodopa in the brain will bring a lot of side effects for health. Thus, a simple and accurate analytical method is indispensable for the determination of levodopa in biological fluids. In more recent decades, various analytical techniques have been used for levodopa detection, such as chemiluminescence, high performance liquid chromatography, fluorescence, and electrochemical sensor [5–8]. In comparison with other reported methods, electroanalytical methods have been received tremendous attention due to their high sensitivity, rapid response, low cost and simplicity in the operation procedure [9–13]. For an electrochemical sensing system, the detection efficiency mainly relies on the electrode materials.

As is generally known, two-dimensional covalent organic frameworks (2D COFs) are a burgeoning class of porous crystalline materials whose backbone is composed entirely of light elements (B, C, N, O, Si) [14,15]. Since the creationary work of Yaghi and co-workers reported in 2005 [16], the COFs materials have shown superior potential in a wide range of applications [17–19]. In comparison with other traditional crystalline porous solids, (i) the strong covalent bonding between the organic building units endows COFs with high chemical and thermal stability; (ii) large surface area and functional groups on the synthesized COFs is beneficial for the interactions with object molecules; (iii) the self-assembled two-dimensional pore channels constructed by the interlayer interactions (π–π stacking) of COFs can accelerate charge

* Corresponding author. Tel./fax: +86-514-87975587.
** Corresponding author. Tel./fax: +86-577-88017535.
E-mail addresses: wangyzu@126.com (Y. Wang), wangyi@wiucas.ac.cn (Y. Wang).
[1] These authors contributed equally to this work.

https://doi.org/10.1016/j.talanta.2020.122072
Received 17 October 2020; Received in revised form 25 December 2020; Accepted 26 December 2020
Available online 2 January 2021

transport to the surface. To some extent, these characteristics also make attractive for COFs to be a potential electrode material. Unfortunately, the poor electrical conductivity of COFs is a blockage for their use as electrochemical sensors.

To address this issue, coupling COFs with other specific conductive materials will be an effective strategy to regulate the limited electrochemical performance (e.g. graphene oxide, and metal nanoparticles) [20–22]. Among these materials, metal nanoparticles (NPs) have been widely used in the electrochemical sensing fields because of their excellent catalytic properties and conductivity [23–27]. Nevertheless, endeavors have been committed to preparing bimetallic NPs with excellent synergistic catalysis properties compared with those of monometallic NPs [28,29], and the combination of bimetallic NPs and COFs has not been reported.

Although many materials with predominant catalytic performances, such as carbon nanotubes, graphene and graphene oxide, metal nanoparticles and nanocomposites and conductive polymers together with carbon paste, glassy carbon, and indium tin oxide electrodes, have been introduced to improve the detectability of electrochemical sensors for levodopa [30–38], most of them have shown various drawbacks in connection with low effective surface, lack of structural design and possibility for surface functionalization. Hence, there is a growing demand for new materials with high surface areas and diverse structures to face the challenges of ever evolving analytical applications. Herein, we presented the developing of a novel composite material based on bimetallic nanoparticles and COF, which was employed to modify a glassy carbon electrode and to manufacture an amperometric sensor to determine levodopa. Parameters that affect the analytical performance were systematically investigated prior to its determination with differential pulse voltammetry. The AgCo/TAPB-DMTP–COF–based electrochemical sensor can be used for the precise detection of levodopa in human blood serum and urine, demonstrating its extensive promising applications in practical measurements.

2. Experimental section

2.1. Reagents and materials

1,3,5-tris(4-amino-phenyl)benzene (TAPB), 2,5-dimethoxyterephaldehyde (DMTP), silver nitrate ($AgNO_3$), cobalt nitrate ($Co(NO_3)_2 \cdot 6H_2O$), alumina slurry (Al_2O_3), sodium borohydride ($NaBH_4$), methanol, acetic acid, butanol, tetrahydrofuran and 1,4-dioxane were purchased from Sinopharm Chemical Reagent Co., Ltd. (Shanghai, China). 0.10 mol L^{-1} acetate buffer solution (ABS), (pH 4.0–5.8) was prepared by mixing moderate amounts of sodium acetate and acetic acid. Double deionized water (18 MΩ cm^{-1}) was prepared by Milli-Q water purification system (Millipore, Bdfedford, MA, USA). Nitrogen gas (99.999%) was used for purging oxygen in a solution to provide an inert atmosphere.

2.2. Instrumentations

X-ray diffraction (XRD) analysis was obtained with a D8 Advance X-ray diffractometer (Bruker Co., Germany) from 1.5° to 80°. Fourier transform infrared spectroscopy (FTIR) spectra were performed on a Cary 610/670 infrared microspectrometer (Varian, America). X-ray photoelectron spectroscopy (XPS) analyses were taken from in an ESCALAB 250 high-performance electron XPS spectrometer (Thermo Scientific, American). High-resolution transmission electron micrographs (HRTEM) were collected by a FEI Tecnai G2 F30 S-TWIN field-emission transmission electron microscopy (USA). Electrochemical measurements were implemented on a CHI852C electrochemical workstation (Shanghai Chenhua Co., China). In the three-electrode system, the AgCo/TAPB-DMTP-COF modified glassy carbon electrode (GCE) was used as working electrode. The reference electrode was comprised of Ag/AgCl (3.0 mol L^{-1} KCl), and the counter electrode a platinum wire.

2.3. Synthesis of TAPB-DMTP-COF

TAPB-DMTP-COF was prepared based on a previously reported procedure [22]. 1,3,5-tris(4-aminophenyl)benzene (TAPB) (0.03 mmol, 10.5 mg) and 2,5-dimethoxyterephaldehyde (DMTP) (0.045 mmol, 8.7 mg) were combined in a 20 mL borosilicate glass vial with a 1,4-dioxane-butanol-methanol solution (4:4:1 v/v/v, 4.5 mL), and the mixture was sonicated for 10 min at room temperature. Subsequently, 0.5 mL of 12 mol L^{-1} acetic acid was added and the mixture was kept at 70 °C for 24 h. After cooling down to room temperature naturally, the product was treated with tetrahydrofuran and acetone for several times and dried under vacuum at 60 °C overnight.

2.4. Synthesis of AgCo/TAPB-DMTP-COF

Firstly, 0.24 mmoL of $AgNO_3$ and 0.20 mmoL of $Co(NO_3)_2 \cdot 6H_2O$ were dissolved in 5 mL aqueous solution. After vigorously stirring for 30 min at room temperature, 40 mg of TAPB-DMTP-COF was added into the solution and the mixture was stirred for 4 h at 0 °C to impregnate the metal salts. Subsequently, 2.0 mL of 0.1 mol L^{-1} $NaBH_4$ water solution was added dropwise into the above solution, and stirred vigorously at 0 °C for 4 h. After cooling to room temperature, the product was washed with methanol and deionized water for 3 times, and finally dried under vacuum at 60 °C for 12 h.

2.5. Preparation of AgCo/TAPB-DMTP-COF/GCE

Before modification, the bare GCE was polished to a mirror-like surface on the chamois leather with 0.5 and 0.03 μm alumina suspensions, followed by washing with double deionized water and ethanol by sonication, and finally permitted to dry in N_2 blowing. AgCo/TAPB-DMTP-COF (1.0 mg) was dissolved in 1.0 mL of deionized water under ultrasonication to form a homogeneously suspension. Then 5 μL of AgCo/TAPB-DMTP-COF solution was casted on the surface of GCE and the solution was evaporated in a desiccator. The similar approach was also employed to fabricated TAPB-DMTP-COF/GCE and AgCo/GCE.

2.6. Electrochemical measurement

Differential pulse anodic stripping voltammetry (DPV) was performed. The solution of the 0.1 mol L^{-1} of ABS (pH 5.0) containing the appropriate volume of levodopa stock solution was prepared and transferred into an electrochemical cell for a total volume of 10 mL. The DPV were recorded by scanning the potential from 0.1 to 0.8 V vs. Ag/AgCl with a step potential of 10 mV, scan rate of 100 mV s^{-1}, pulse amplitude of 50 mV, pulse width of 1.0 s, sample width of 0.02 s and pulse period of 0.5 s.

3. Results and discussion

3.1. Characterization of materials

For the pure TAPB-DMTP-COF, a spherical-like surface morphology, and type-IV N_2 adsorption-desorption isotherm curve were shown in Figs. S1, S2 in the Supporting Information. The BET surface area and pore volume TAPB-DMTP-COF was calculated to be 2385 m^2 g^{-1}, and 1.27 cm^3 g^{-1}, respectively. The crystalline structure of samples was investigated by the powder XRD technique. As illustrated in Fig. 1A, six characteristic peaks of TAPB-DMTP-COF at 2.79°, 4.84°, 5.60°, 7.39°, 9.73° and 25.42° were assigned to the (100), (110), (200), (210), (220) and (001) plane, respectively, which were in good consistence with the previous literature [21]. As for AgCoNPs, peaks detected at 2θ = 38.2°, 44.4°, 64.6° and 77.6° can be corresponded to the reflections from Ag (111), Co (200), Ag (220) and Co (311) planes, respectively [39], After

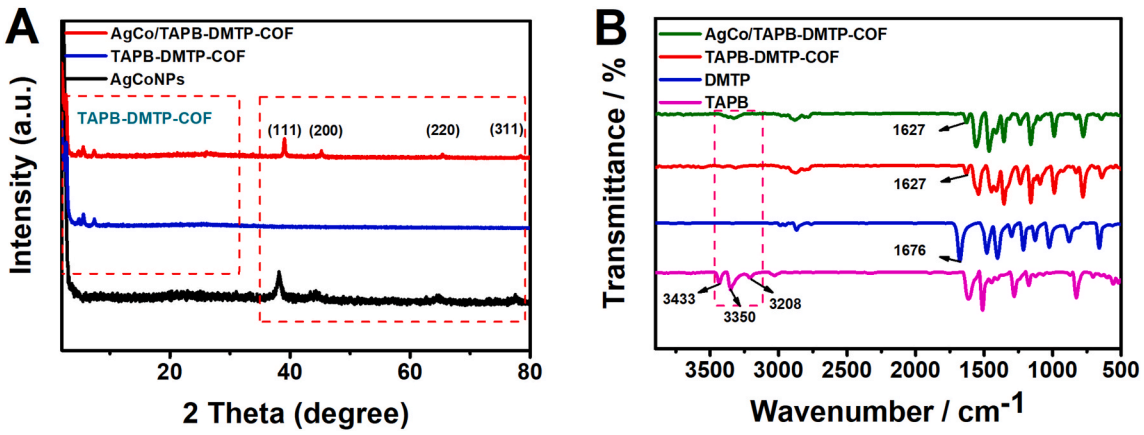

Fig. 1. (A) XRD patterns of TAPB-DMTP-COF, AgCoNPs and AgCo/TAPB-DMTP-COF composites. (B) FTIR patterns of TAPB, DMTP, TAPB-DMTP-COF and AgCo/TAPB-DMTP-COF composites.

the immobilization of AgCoNPs on the TAPB-DMTP-COF matrix, intensity and positions of diffraction peaks of AgCo/TAPB-DMTP-COF was almost identical to the pure TAPB-DMTP-COF, which suggested that the integrity of AgCo/TAPB-DMTP-COF structure was retained during the immobilization of AgCoNPs via the post-reduction approach. Fourier transform infrared (FTIR) spectra of TAPB, DMTP, TAPB-DMTP-COF and AgCo/TAPB-DMTP-COF composites were shown in Fig. 2B. Three peaks at 3433, 3350, and 3208 cm^{-1} were the characteristics for the stretching vibration of N–H of TAPB. The intensive peak in 1676 cm^{-1} was related to the C═O stretching vibration of DMTP. For TAPB-DMTP-COF, an obvious peak of C═N bonds was appeared at 1627 cm^{-1}, suggesting that a condensation reaction has occurred [40]. A similar FTIR spectrum was observed for AgCo/TAPB-DMTP-COF, which were consistent with the previous powder XRD results.

To research the chemical state and composition, TAPB-DMTP-COF and AgCo/TAPB-DMTP-COF were characterized by X-ray photoelectron spectroscopy (XPS). As shown in Fig. 2A, the XPS survey spectrum of the TAPB-DMTP-COF indicated the existence of C, N, O elements. Additionally, Ag and Co elements emerged in the AgCo/TAPB-DMTP-COF composite. From the curve of TAPB-DMTP-COF (Fig. 2B), two distinct peaks at 401.5 and 398.8 eV were ascribed to the $–NH_2$ and C═N groups, respectively. After the immobilization of AgCoNPs on TAPB-DMTP-COF, the binding energy of $–NH_2$ had a significant increase. The reason for the shift of 5.4 eV can be explained that there was

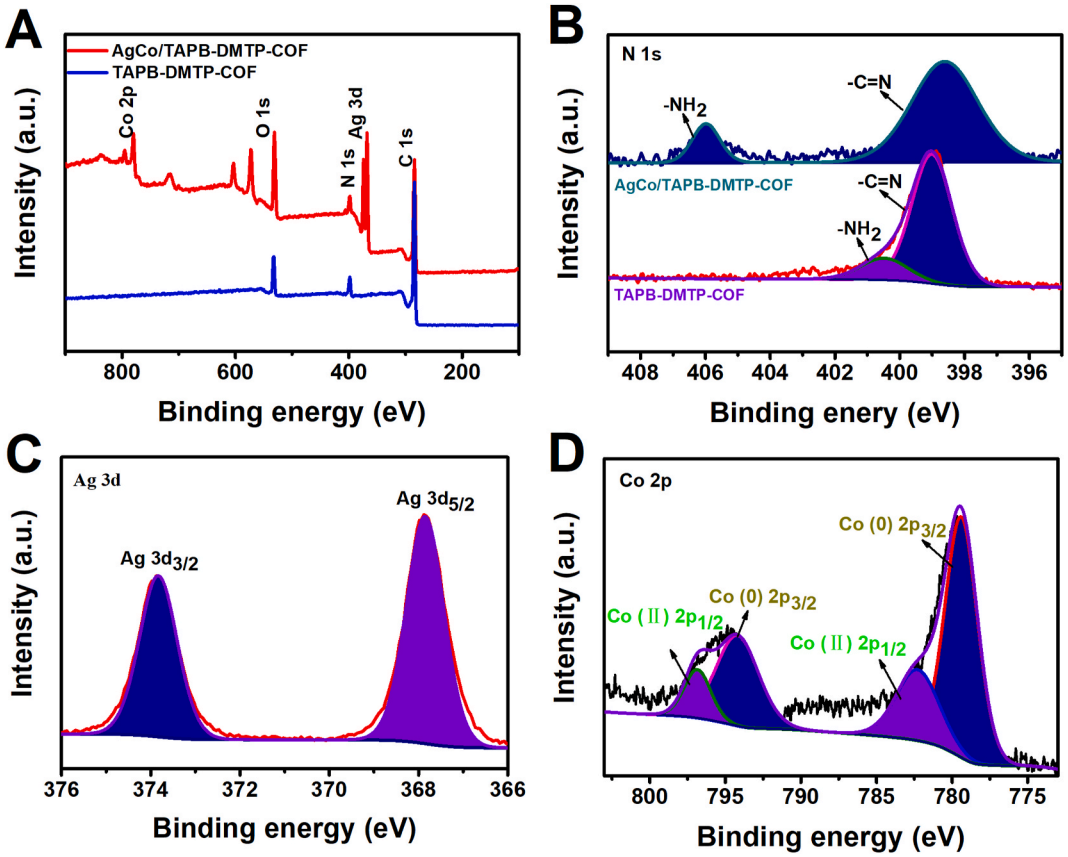

Fig. 2. (A) XPS survey spectrum of TAPB-DMTP-COF and AgCo/TAPB-DMTP-COF. (B) High resolution N 1 s region in the XPS of TAPB-DMTP-COF and AgCo/TAPB-DMTP-COF. Ag 3d (C) and Co 2p (D) spectra of AgCo/TAPB-DMTP-COF.

a strong interaction between bimetal ions and COF. The Ag 3d spectrum appeared one pair of peaks (Ag $3d_{3/2}$/Ag $3d_{5/2}$) at 373.8 and 367.8 eV, which were assigned to Ag^0 (Fig. 2C) [41]. Meanwhile, The approximate difference of the 3d doublet of Ag was 6.0 eV, confirming the reduction of Ag^+ ions as well [42]. In Fig. 2D, the 794.2 and 779.5eV belonged to the Co^0 $2p_{3/2}$ and Co^0 $2p_{1/2}$, indicating the formation of metallic Co^0 in the composite [43]. In addition, the peaks located at 797.1 eV and 782.3 eV were corresponding to the Co (II) $2p_{3/2}$ and Co (II) $2p_{1/2}$, owing to the incomplete reduction of cobalt.

The high-resolution transmission electronmicroscopy (HRTEM) was implemented to recognize the morphology structure of the composite. Fig. 3a confirmed that AgCoNPs with small sizes have been dispersedly immobilized on the TAPB-DMTP-COF. As shown in Fig. 3b, the typical lattice fringes were 0.235 and 0.205 nm, which agree well with the lattice planes of Ag (111) and Co (111), respectively [44]. Selected area electron diffraction (SAED) image, given in Fig. 3b inset, clearly displayed the lamellar structure of the AgCo/TAPB-DMTP-COF composite. Moreover, with the purpose of further investigating the elemental distribution and composition of AgCo/TAPB-DMTP-COF, the elemental mapping and energy-dispersive X-ray spectroscopy (EDX) were analyzed. Fig. 3(d–h) showed that C, N, O, Ag, and Co elements were distributed throughout AgCo/TAPB-DMTP-COF composite, indicating that AgCoNPs were incorporated into the TAPB-DMTP-COF. The peaks of Ag, Co, C, N, O and C appeared in Fig. 3i, which were related to the sample of AgCo/TAPB-DMTP-COF and copper mesh.

3.2. Electrochemical properties of AgCo/TAPB-DMTP-COF/GCE

The EIS measurement was implemented to investigate the charge transfer process in the interface of the modified electrode and electrolyte. A typical impedance spectrum is consisted of a small semicircle part at high frequencies and a straight line part at low frequencies. This semicircle corresponds to the electron-transfer limited process and its diameter is equal to the charge transfer resistance (Rct) [45]. The EIS curves of stepwise modification process were shown in Fig. 4A. It can be observed that the Rct value of 212 Ω for bare GCE increased to 425 Ω after the immobilization of TAPB-DMTP-COF, which may be ascribed to the low intrinsic conductivity that resulted in poor electron transfer at the electrode surface. Rct values decreased distinctly after the bare GCE was modified with AgCoNPs (106 Ω) and AgCo/TAPB-DMTP-COF (175 Ω), suggesting the cooperation of AgCoNPs TAPB-DMTP-COF greatly accelerates electron transfer speed between the electrolyte and electrode interface. The electrical equivalent circuit model was described in Fig. 4A inset. The model consists of the electrode surface resistance (Rs), Rct, Warburg impedance (Zw) and the constant phase angle element (CPE). Among them, Zw represents the impedance is a result of the diffusion layer between the bulk solution and the electrode surface. For the AgCo/TAPB-DMTP-COF/GCE, there is a small half semicircle

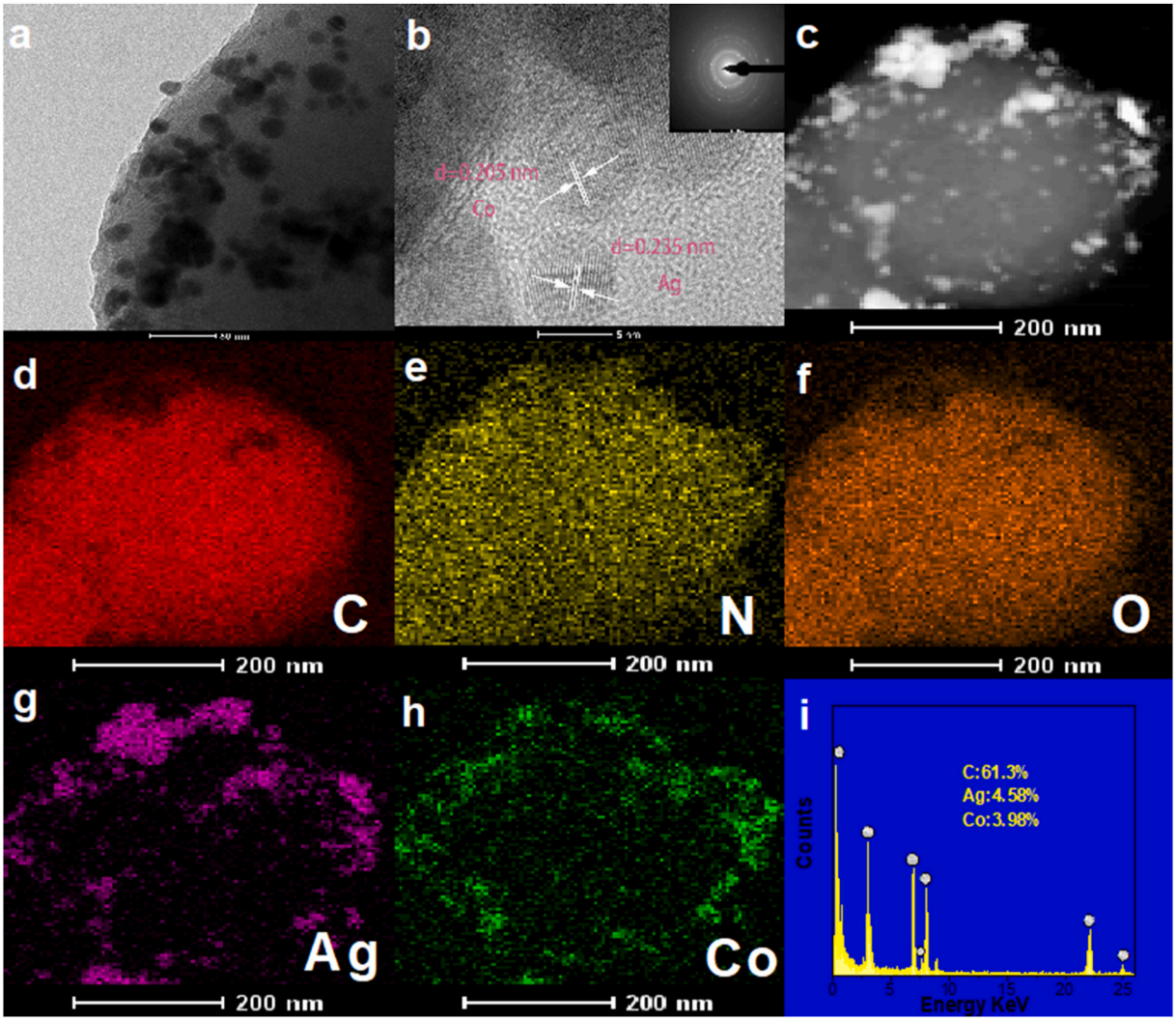

Fig. 3. HRTEM images of AgCo/TAPB-DMTP-COF with diverse magnified folds (a and b). Inset: SAED pattern of AgCo/TAPB-DMTP-COF. Elemental mapping images (c–h) and EDX spectrum (i) of the AgCo/TAPB-DMTP-COF composite.

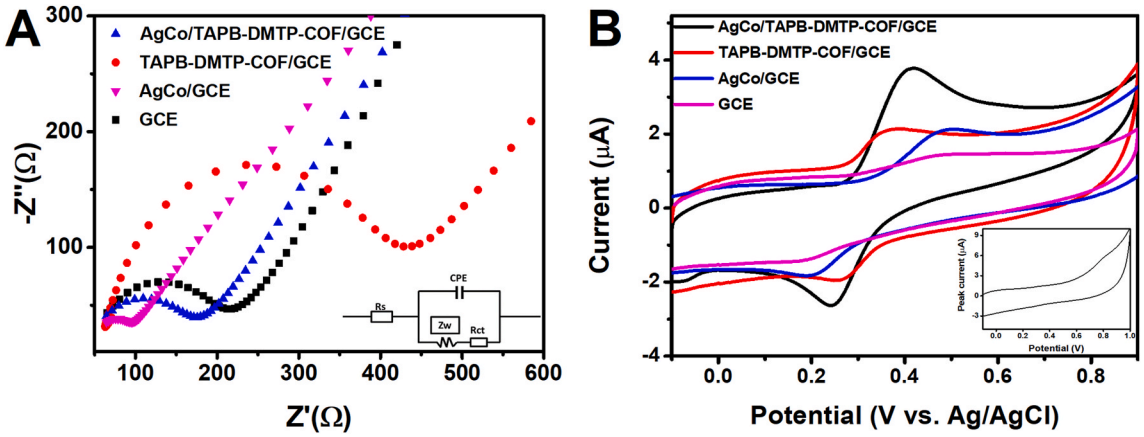

Fig. 4. (A) EIS of different modifed electrodes in 5.0 mmol L^{-1} $Fe(CN)_6^{3-/4-}$ solution containing 0.10 mol L^{-1} KCl. The equivalent circuit is inserted. (B) CVs at the different modifed electrodes in 0.10 mol L^{-1} ABS (pH 5.0) with the presence of 50 μmol L^{-1} levodopa at the scan rate of 0.1 V s^{-1}. Inset: CVs of levodopa at the AgCo/TAPB-DMTP-COF/GCE in 0.10 mol L^{-1} ABS (pH 5.0) with the absence of levodopa.

observed at the low-frequency region, which demonstrates that the influence of the Warburg impedance is low. It also shows that the proposed modified electrode has slightly capacitive behavior due to the AgCoNPs in the electrode composite. Furthermore, electrochemical behaviors of diverse electrodes toward the levodopa were measured by CVs experiments. No redox peaks were found in the inset of Fig. 4B, indicating the AgCo/TAPB-DMTP-COF composite was non-electroactive at the implemented potential. From Fig. 4B, all CV curves displayed a pair of redox peaks after the introduction of levodopa. The bare GCE was active for levodopa solution, but the response towards levodopa was quite weak. In contrast, the anodic peak current of AgCo/TAPB-DMTP-COF/GCE (I = 3.089 μA) was about 5 times higher than that of bare electrode (I = 0.623 μA). Obviously, the best electrochemical response was attributed to the synergistic amplification effect of AgCoNPs and TAPB-DMTP-COF: Firstly, the attractive porous structure of TAPB-DMTP-COF can provide the higher electrode active surface area.

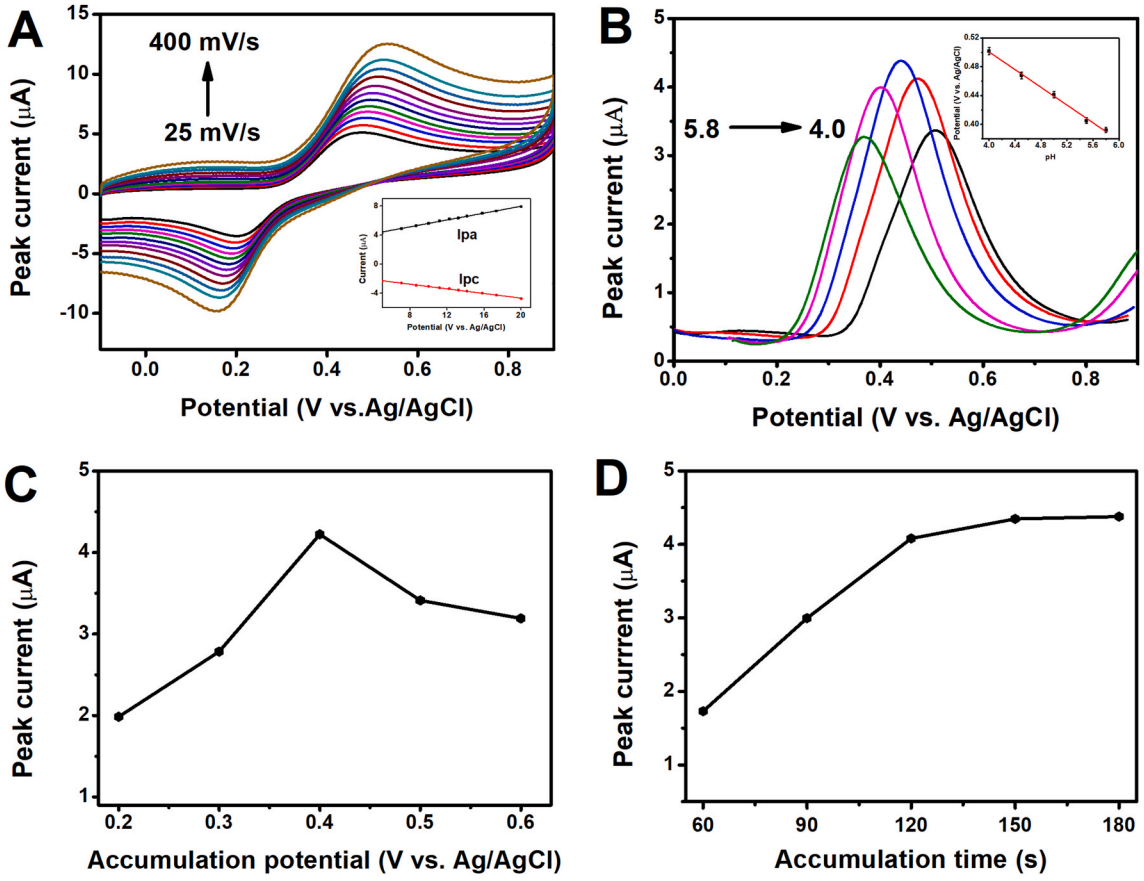

Fig. 5. (A) CVs for 50 μmol L^{-1} levodopa at AgCo/TAPB-DMTP-COF/GCE in 0.10 mol L^{-1} ABS (pH 5.0) at various scan rates (25, 50, 75, 100, 125, 150, 175, 200, 250, 300, 400 mV · s^{-1}). Inset: the linear relationship between redox peak currents and square root of scan rates. (B) DPV of 50 μmol L^{-1} levodopa at AgCo/TAPB-DMTP-COF/GCE in 0.1 mol L^{-1} ABS with different pH values (4.0, 4.5, 5.0, 5.5 and 5.8). Inset: Dependence of solution pH on the reduction potential. Effects of deposition accumulation potential (C) and time (D) on the peak current in 0.10 mol L^{-1} ABS containing 50 μmol L^{-1} levodopa.

Secondly, AgCoNPs have favorable conductivity and catalytic property to improve the oxidation process toward levodopa. Thirdly, levodopa molecule can be absorbed onto the surface of modified electrode through the interaction of π-π stacking. In addition, the anodic peak (ΔEp) decreased from 301 mV to 155 mV after the AgCo/TAPB-DMTP-COF/GCE coated on the surface of GCE, reflecting that this modified electrode had a rapid electron transfer speed. Thus, the above results have confirmed that AgCo/TAPB-DMTP-COF has great potential to serve as an electrochemical sensor with excellent performance.

3.3. Optimization of experimental parameters

A univariate optimization study was performed to establish the optimized experimental conditions. It was defined as a non-linear optimization with no constraint, and only one decision variable in the optimization problem.

min f(x), w.r.t x, subject to a < x < b. where f(x) represents objective function, w.r.t x denotes decision variable, a and b are constraint. In this work, the optimizations of the electrochemical parameters mainly include scan rate, solution pH, accumulation potential and time.

In order to account for the electrochemical mechanism of levodopa on AgCo/TAPB-DMTP-COF modified electrode, the influence of different scan rates was investigated. Fig. 5A showed the CVs of AgCo/TAPB-DMTP-COF/GCE with the scan rate in the range of 25–350 mV · s^{-1}. As described in Fig. 5B inset, anodic and cathodic peaks current were linearly related to the square root of scan rate. Linear regression equations were expressed as I_{pa} (μA) = 0.2362 $V^{1/2}$ ($mV^{1/2}$ $s^{-1/2}$) + 3.244 ($R^2 = 0.998$), and I_{pc} (μA) = − 0.1596 $V^{1/2}$ ($mV^{1/2}$ $s^{-1/2}$) - 1.4779 ($R^2 = 0.996$), which indicated that the electrocatalytic oxidation process of levodopa is a diffusion controlled reaction.

Optimizations of electrochemical reaction conditions for the fabrication of the electrochemical sensor are crucial to achieving a better analytical performance. The effect of pH value on electrochemical detection of levodopa was explored by DPV in the range of 4.0–5.8. As shown in Fig. 5B, the anodic peak current gradually increased with rising pH until pH 5.0. Subsequently, the current responses decreased quickly. Thus, the pH of 5.0 was chosen to act as a as the optimal experimental condition to detect levodopa. The inset of Fig. 5B displayed that the reduction potential shifted negatively with the increase of pH values, indicating that the proton was involved in the electrode reaction. The linear relationship between the anodic peak current and pH value can be expressed by the regression equation was E_{pc} (μA) = 0.7477–0.0617 pH (R^2 = 0.997). The slope of 61 mV · pH^{-1} was approximated to the anticipated Nernstian value of 59 mV · pH^{-1}, which showed the number of the protons were quite equivalent to the electron number in the electrode reaction of levodopa. According to $\Delta Ep = 2.3RT/\alpha nF$, where α and n represent the charge transfer coefficient and the transferred electron number, respectively. For a quasi-reversible process, the value of α is assumed to be 0.5. Therefor, n was calculated to be 1.92, indicating the electrocatalytic oxidation process of levodopa was two electrons transferred. Considering accumulation is an important parameter to improve the sensitivity and selectivity of the sensor, the accumulation potential and time optimization were performed by DPV. Fig. 4C demonstrated the impact of accumulation potential on the current responses. As the potential value increased from 0.2 to 0.4 V, the peak currents gradually enhanced. The maximum value was 0.4 and then reduced. Therefor, the accumulation potential selected for use in the further research was 0.4 V. The deposition time was also optimized and the result was displayed in Fig. 5D. It was obviously seen that the current responses were improved sharply when the accumulation time was enhanced from 60 to 120 s. Subsequently, the current responses reached a plateau after 120 s, reflecting the saturated binding of levodopa on the electrode surface. Therefor, the accumulation time was 120 s.

3.4. Analytical performance of the electrochemical sensor

Under the optimized experimental conditions, the electrochemical performance of AgCo/TAPB-DMTP-COF/GCE was researched by DPV. Fig. 6A portrayed the oxidation peak currents enhanced with concentration of levodopa. There were two different linear relationships over two intervals in 0.01–10.00 μmol L^{-1} and 10.00–100 μmol L^{-1}, as seen in Fig. 6B inset. Linear equations were calculated as:

0.01–10.0 μmol L^{-1}: I_{pa} (μA) = 0.1572C (μmol L^{-1}) + 0.3974 (R^2 = 0.999)

10.0–100.0 μmol L^{-1}: I_{pa} (μA) = 0.0635C (μmol L^{-1}) + 1.191 (R^2 = 0.997)

Two slopes of the standard curve in our study may be explained as follows: At the first linear part, small amounts of levodopa molecules can be quickly converted into product at the electrode surface, resulting in a higher sensitivity towards levodopa determination. At the second linear part, accompanying with the concentrations of levodopa increasing, the modified electrode surface was covered by a large amount of levodopa, and the mass transfer resistance was therefore enlarged. Hence, the sensitivity will be undoubtedly decreased at the second interval. Compared with previously reported electrode materials for levodopa testing (Table 1) [30–38], the proposed AgCo/TAPB-DMTP–COF–based sensor showed prominent electrochemical property with the lowest limit of detection (LOD) among them. The LOD was determined to be 0.002 μmol L^{-1} with a signal-to-noise (S/N) ratio of 3. This outstanding levodopa detection efficiency may be attributed to the following factors: (1) the large specific surface area of TAPB-DMTP-COF could effectively improve the current response for levodopa detection. (2) levodopa can be adsorbed onto the electrode surface through π-π stacking and hydrogen-bond interaction between the AgCo/TAPB-DMTP-COF and analyte; (3) The AgCo/TAPB-DMTP-COF with excellent electroconductibility could accelerate the electron transfer towards the surface of the electrode.

3.5. Reproducibility, stability and interference studies

The reproducibility of the AgCo/TAPB-DMTP–COF–based sensor was also confirmed by detecting 20 μmol L^{-1} levodopa at seven independent electrodes. From Fig. 7A, the relative standard deviation (RSD) was computed to be 4.0%, which implied that the proposed sensor possessed a prominent reproducibility. After continuous ten determinations by DPV on one electrode, the RSD value was 3.2%, suggesting the excellent repeatability of the sensor (Fig. 7B). In order to assess the stability of AgCo/TAPB-DMTP-COF/GCE, the peak current was investigated by DPV. Almost no distinct change in current responses was observed after 100 cycles and the current response kept 91% of the original value. The excellent stability of the sensor may emanate from the bonding strength between components of the 2D layers and the interlayer force [46].

Anti-interference performance of the sensor played an important role for evaluating the property of electrochemical analysis application. It was well known that the presence of some similar analytes may impact the current responses, such as ascorbic acid, glucose, uric acid, and its enantiomers. The level of tolerance for foreign species was determined by a variation in current intensity within ±5%. The result indicated that Mg^{2+}, Cu^{2+}, Pb^{2+}, Ca^{2+}, K^{+}, Na^{+}, Cl^{-}, NO_3^{-}, CO_3^{2-}, NH_4^{+} and SO_4^{2-} with 1000-fold of concentrations had inappreciable interference on the electrochemical signals. No distinct response change was found by the introduction of 100-fold concentrations of glucose, sucrose, fructose, lactose, folic acid, paracetamol, L-cysteine alanine and adenine, 50-fold concentrations of ascorbic acid, uric acid, dopamine, adrenaline, noradrenaline, catechol, thymol and rutin. All these results suggested that the AgCo/TAPB-DMTP–COF–based sensor exhibited a great selectivity for levodopa determination, which could be due to the presence of abundant channels in TAPB-DMTP-COF can permit the size and shape-selectivity over the guests.

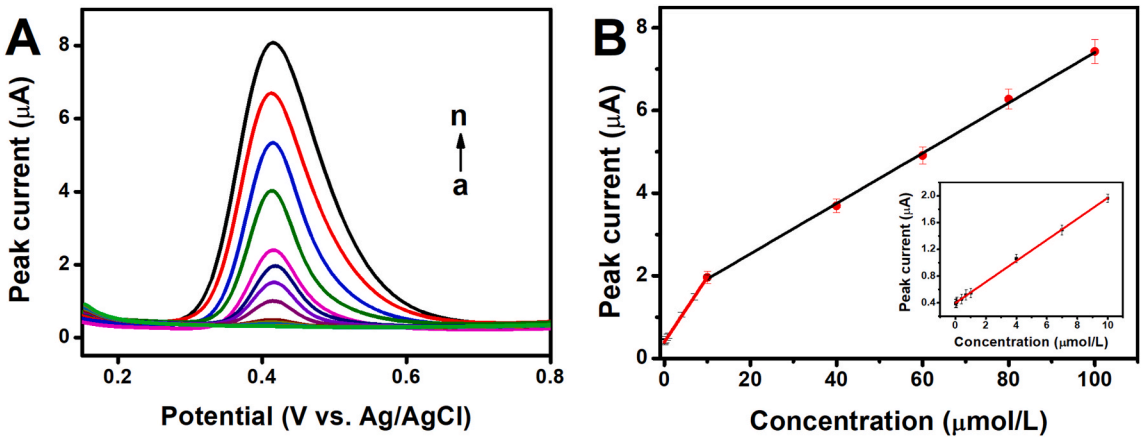

Fig. 6. (A) DPVs at the AgCo/TAPB-DMTP-COF of levodopa with different concentrations in the pH 5.0 ABS. (from a to n: 0.01, 0.04, 0.07, 0.1, 0.4, 0.7, 1.0, 4.0, 7.0, 10, 40, 60, 80, 100 μmol L^{-1}). (B) The calibration plot of peak current versus levodopa concentration. Inset: the trend of current intensity when levodopa concentrations are low.

Table 1
Comparison of the proposed method for the determination of levodopa with other reported techniques.

Electrode substrate	Linear range (μmol L^{-1})	Detection limit (μmol L^{-1})	Reference
rGO/GCE	2–100	1.13	[30]
TNF/GO/GCE	0.3–60	0.016	[31]
AuNP-CMC-xGnP/GCE	5–50	0.50	[32]
MWCNT-PAH/GCE	2–27	0.84	[33]
CP-TNMCPE	0.1–100	0.069	[34]
3,4′-AAZCPE	0.05–20	0.035	[35]
ZnO NWAs/GF/ITO	0.01–0.5	0.05	[36]
MoS_2-graphene/ITO	5–60	0.3	[37]
$Co(DMG)_2ClPy$/MWCNT/BPPG	3–100	0.86	[38]
AgCo/TAPB-DMTP-COF/GCE	0.01–100	0.002	This Work

rGo: reduced graphene oxide, TNF: titanium dioxide nanofiber, GO: graphite oxide paste, CMC: carboxymethylcelullose, xGnP: exfoliated graphite nanoplatelets, MWCNT: Multiwalled carbon nanotubes, PAH: allylamine hydrochloride, CP: cobalt porphyrin, TNMCPE: TiO_2 nanoparticles paste electrode, 3,4′-AAZ: 5-(4′-amino-3′-hydroxy-biphenyl-4-yl)-acrylic acid, CPE: carbon paste electrode, ZnO NWAs: ZnO nanowire arrays, GF: graphene foam, ITO: indium tin oxide, $Co(DMG)_2ClPy$: chloro(pyridine)bis(dimethylglyoximato)cobalt(III), BPPG: basal plane pyrolytic graphite.

3.6. Real sample analyses

The feasibility and accuracy of the AgCo/TAPB-DMTP–COF–based sensor for levodopa determination in real samples was assessed by the standard addition approach. Diverse concentrations of levodopa were added into 50-fold diluted human urine and blood serum samples, which obtained from the affiliated hospital of Yangzhou University. Then, the designed sensor was used to detect the concentration of levodopa. As shown in Table 2, it was clearly seen that the range of recovery of spiked samples was 98.0–104.2%. Meanwhile, RSD values of five times paralleled detection were obtained from 1.6 to 3.9%. These test results

Table 2
Determination of levodopa in human urine and blood serum samples (n = 5).

Samples	Added (μmol · L^{-1})	Found (μmol L^{-1})	Recovery (%)	R.S.D. (%)
Human Urine	0.00	ND	–	–
	10.00	9.9 ± 0.1	99.0	1.6
	30.00	31.2 ± 0.1	103.9	3.1
	50.00	52.1 ± 0.2	104.2	3.9
Human blood serum	0.00	ND	–	–
	10.00	10.3 ± 0.1	103.2	1.9
	30.00	29.6 ± 0.1	98.6	2.4
	50.00	49.0 ± 0.1	98.0	3.4

ND: Not detected.

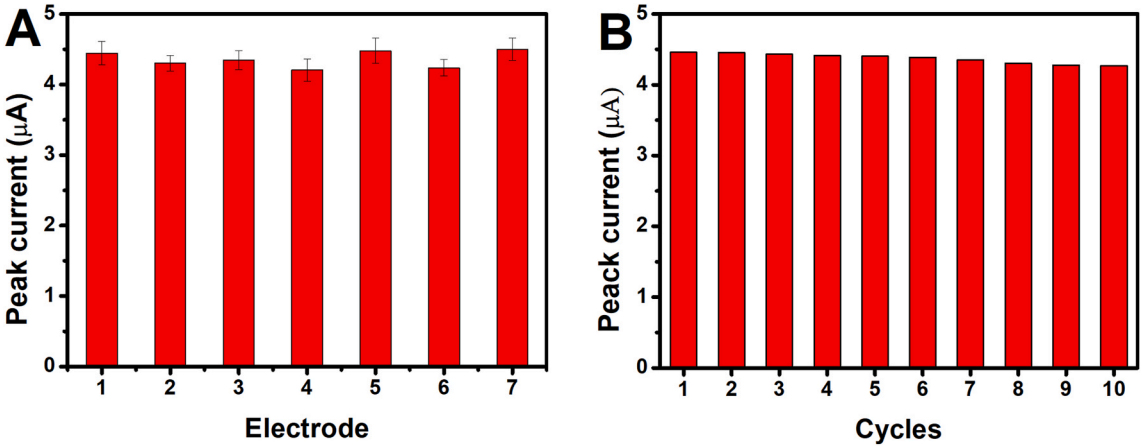

Fig. 7. (A) Reproducibility of the AgCo/TAPB-DMTP–COF–based sensor at the independent electrodes in the existence of 50 μmol L^{-1} levodopa. (B) Repeatability of the proposed sensor on one electrode in the existence of 50 μmol L^{-1} levodopa.

demonstrated that the prepared AgCo/TAPB-DMTP–COF–based sensor was feasible and practical for levodopa analysis in real samples.

4. Conclusion

In summary, a novel bimetallic functionalized COF composite (AgCo/TAPB-DMTP-COF) was synthesized via a simple reduction method, which excellent electrocatalytic activity toward levodopa voltammetric determination. The optimized electrochemical parameters such as scan rate, solution pH, accumulation potential and time were achieved. As expected, the AgCo/TAPB-DMTP-COF based electrochemical sensor shows wider linear range, lower detection limit, low interference, and remarkable selectivity. It also has a good electrochemical stability during the levodopa oxidation process. The excellent analytical performance can be ascribed to the high electroactive surface area of COFs and great electrical conductivity of bimetallic NPs. Furthermore, it is the first time that the combination of COFs and bimetallic NPs was utilized as an electrode material in electrochemical domain. Significantly, the sensor mentioned in this work was capable to detect trace levels of levodopa in human urine and human blood serum samples with satisfying properties. Our work exploits a new approach to COFs-based multifunctional sensor, which has great potential to apply for clinical diagnosis of levodopa in the future.

Credit author statement

Xin Sun: synthesized the AgCo/TAPB-DMTP-COF composites and applied this novel material to detect levodopa in real samples. Na Wang: optimized the experimental parameters during the levodopa detection, and also checked the grammar error existed in the manuscript. Yao Xie: synthesized the TAPB-DMTP-COF composites. Huacong Chu: checked the grammar error existed in the manuscript. Yang Wang: provides the idea of increasing conductivity of TAPB-DMTP-COF via bimetallic nanoparticles. Furthermore, all the works are guided by Pro. Wang. Yi Wang: reviewed this paper before it was submitted to the journal and gave much important advice to make this paper better.

Declaration of competing interest

The authors declare that they have no known competing financial interests or personal relationships that could have appeared to influence the work reported in this paper.

Acknowledgements

This work was supported by the National Natural Science Foundation of China (21205103), Jiangsu Provincial Nature Foundation of China (BK2012258), Decision-making Program of Shanghai Jiao Tong University (JCZXSJB2019-016), and a project funded by the Priority Academic Program Development of Jiangsu Higher Education Institutions (PAPD).

Appendix A. Supplementary data

Supplementary data to this article can be found online at https://doi.org/10.1016/j.talanta.2020.122072.

References

[1] Z.J. Yang, X.C. Huang, J. Li, Y.C. Zhang, S.H. Yu, Q. Xu, X.Y. Hu, Carbon nanotubes-functionalized urchin-like In_2S_3 nanostructure for sensitive and selective electrochemical sensing of dopamine, Microchim. Acta 177 (2012) 381–387.
[2] J.A.D. Silva, F. Tecuapetla, V. Paixao, R.M. Costa, Dopamine neuron activity before action initiation gates and invigorates future movements, Nature 554 (2018) 244–248.
[3] K.Y. Goud, C. Moonla, R.K. Mishra, C. Yu, R. Narayan, I. Litvan, J. Wang, Wearable electrochemical microneedle sensor for continuous monitoring of levodopa: toward Parkinson management, ACS Sens. 4 (2019) 2196–2204.
[4] Y.L. Chen, X. Sun, S. Biswas, Y. Xie, Y. Wang, X.Y. Hu, Integrating polythiophene derivates to PCN-222(Fe) for electrocatalytic sensing of L-dopa, Biosens. Bioelectron. 141 (2019) 111470.
[5] W.W. He, X.W. Zhou, J.Q. Lu, Simultaneous determination of benserazide and levodopa by capillary electrophoresis–chemiluminescence using an improved interface, J. Chromatogr. A 1131 (2006) 289–292.
[6] F. Belal, F. Ibrahim, Z.A. Sheribah, H. Alaa, Micellar HPLC-UV method for the simultaneous determination of levodopa, carbidopa and entacapone in pharmaceuticals and human plasma, J. Chromatogr. B 1091 (2018) 36–45.
[7] M.F. Bergamini, A.L. Santos, N.R. Stradiotto, M.V.B. Zanoni, A disposaable electrochemical sensor for the rapid determination of levodopa, J. Pharmaceut. Biomed. 39 (2005) 54–59.
[8] M.R. Ajmal, T.I. Chandel, P. Alam, N. Zaidi, M. Zaman, S. Nusrat, M.V. Khan, M. K. Siddiqi, Y.E. Shahein, M.H. Mahmoud, G. Badr, R.H. Khan, Fibrillogenesis of human serum albumin in the presence of levodopa - spectroscopic, calorimetric and microscopic studies, Int. J. Biol. Macromol. 94 (2017) 301–308.
[9] Q. Xu, X.J. Li, Y.E. Zhou, H.P. Wei, X.Y. Hu, Y. Wang, Z.J. Yang, An enzymatic amplified system for the detection of 2,4-dichlorophenol based on graphene membrane modified electrode, Anal. Methods 4 (2012) 3429–3435.
[10] C. Hou, Q. Xu, L. Yin, X. Hu, Metal-organic framework templated synthesis of Co_3O_4 nanoparticles for direct glucose and H_2O_2 detection, Analyst 137 (2012) 5803–5808.
[11] J. Chen, Q. Xu, Y. Shu, X. Hu, Synthesis of a novel Au nanoparticles decorated Ni-MOF/Ni/NiO nanocomposite and electrocatalytic performance for the detection of glucose in human serum, Talanta 184 (2018) 136–142.
[12] C. Yang, X.L. Cui, K. Wang, Y. Cao, C.Y. Wang, X.Y. Hu, A non-enzymatic glucose sensor based on Pd-Fe/Ti nanocomposites, Int. J. Electrochem. Sci. 12 (2017) 5492–5502.
[13] Y.L. Chen, W. Huang, K. Chen, T. Zhang, Y. Wang, J. Wang, Facile fabrication of electrochemical sensor based on novel core-shell PPy@ZIF-8 structures: enhanced charge collection for quercetin in human plasma samples, Sensor. Actuator. B Chem. 290 (2019) 434–442.
[14] Y. Yusran, H. Li, X. Guan, Q. Fang, S. Qiu, Covalent organic frameworks for catalysis, Energy Chem 2 (2020) 100035.
[15] T. Zhang, C. Gao, W. Huang, Y. Chen, Y. Wang, J. Wang, Covalent organic framework as a novel electrochemical platform for highly sensitive and stable detection of lead, Talanta 188 (2018) 578–583.
[16] A.P. Cote, A.I. Benin, N.W. Ockwig, M. OKeeffe, A.J. Matzger, O.M. Yaghi, Porous, crystalline, covalent organic frameworks, Science 310 (2005) 1166–1170.
[17] N. Huang, X. Chen, R. Krishna, D. Jiang, Two-dimensional covalent organic frameworks for carbon dioxide capture through channel-wall functionalization, Angew. Chem. Int. Ed. 54 (2015) 2986–2990.
[18] Y. Yuan, Y. Yang, G. Zhu, Multifunctional porous aromatic frameworks: state of the art and opportunities, Energy Chem 2 (2020) 100037.
[19] S.S. Han, H. Furukawa, O.M. Yaghi, W.A. Goddard, Covalent organic frameworks as exceptional hydrogen storage materials, J. Am. Chem. Soc. 130 (2008) 11580, 11580.
[20] F. Monehzadeh, Z. Rafiee, Application of GO/COF as a novel, efficient and recoverable catalyst in the Knoevenagel reaction, Appl. Organomet. Chem. 34 (2020) 5631.
[21] Y. Xie, T. Zhang, Y.L. Chen, Y. Wang, L. Wang, Fabrication of core-shell magnetic covalent organic frameworks composites and their application for highly sensitive detection of luteolin, Talanta 213 (2020) 120843.
[22] X. Shi, Y. Yao, Y. Xu, K. Liu, G. Zhu, L. Chi, G. Lu, Imparting catalytic activity to a covalent organic framework material by nanoparticle encapsulation, ACS Appl. Mater. Interfaces 9 (2017) 7481–7488.
[23] M. Wang, W. Zhang, X. Zheng, P. Zhu, Antibacterial and catalytic activities of biosynthesized silver nanoparticles prepared by using an aqueous extract of green coffee bean as a reducing agent, RSC Adv. 7 (2017) 12144–12149.
[24] X. Tan, Z. Zhang, T. Cao, W. Zeng, T. Huang, G. Zhao, Control assembly of pillar 6 arene-modified Ag nanoparticles on covalent organic framework surface for enhanced sensing performance toward paraquat, Acs Sustain. Chem. Eng. 7 (2019) 20051–20059.
[25] R. Wang, Y. Yao, M. Shen, X. Wang, Green synthesis of Au@Ag nanostructures through a seed-mediated method and their application in SERS, Colloids Surf., A 492 (2016) 263–272.
[26] J. Han, P. Fang, W. Jiang, L. Li, R. Guo, Ag-nanoparticle-loaded mesoporous silica: spontaneous formation of Ag nanoparticles and mesoporous silica SBA-15 by a one-pot strategy and their catalytic applications, Langmuir 28 (2012) 4768–4775.
[27] J. Han, M. Wang, Y. Hu, C. Zhou, R. Guo, Conducting polymer-noble metal nanoparticle hybrids: synthesis mechanism application, Prog. Polym. Sci. 70 (2017) 52–91.
[28] M. Janyasupab, C.W. Liu, Y. Zhang, K.W. Wang, C.C. Liu, Bimetallic Pt-M (M = Cu, Ni, Pd, and Rh) nanoporous for H2O2 based amperometric biosensors, Sensor. Actuator. B Chem. 179 (2013) 209–214.
[29] F. Wen, Y. Zhang, J. Tan, Z. Zhou, M. Zhu, S. Yin, H. Wang, Pt-Pd co-electrodeposited nitrogenous loofah sponge as efficient pH-universal electrocatalyst for hydrogen evolution reaction, J. Electroanal. Chem. 822 (2018) 10–16.
[30] S.Y. Yi, J.H. Lee, H.G. Hong, A selective determination of levodopa in the presence of ascorbic acid and uric acid using a glassy carbon electrode modified with reduced graphene oxide, J. Appl. Electrochem. 44 (2014) 589–597.

[31] M. Arvand, N. Ghodsi, Electrospun TiO_2 nanofiber/graphite oxide modified electrode for electrochemical detection of L-DOPA in human cerebrospinal fluid, Sensor. Actuator. B Chem. 204 (2014) 393–401.
[32] T.R. Silva, A. Smaniotto, I.C. Vieira, Exfoliated graphite nanoplatelets and gold nanoparticles based electrochemical sensor for determination of levodopa, J. Solid State Electrochem. 22 (2018) 1277–1287.
[33] O.F.F. H.H. Takeda, T.A. Silva, B.C. Janegitz, F.C. Vicentini, L.H.C. Mattoso, Electrochemical sensing of levodopa or carbidopa using a glassy carbon electrode modified with carbon nanotubes within a poly(allylamine hydrochloride) film Anal. Methods 8 (2016) 1274–1280.
[34] M.M. Ardakani, Z. Taleat, A. Khoshroo, H. Beitollahi, H. Dehghani, Electrocatalytic oxidation and voltammetric determination of levodopa in the presence of carbidopa at the surface of a nanostructure based electrochemical sensor, Biosens. Bioelectron. 35 (2012) 75–81.
[35] E. Molaakbari, A. Mostafavi, H. Beitollahi, R. Alizadeh, Synthesis of ZnO nanorods and their application in the construction of a nanostructure-based electrochemical sensor for determination of levodopa in the presence of carbidopa, Analyst 139 (2014) 4356–4364.
[36] H.Y. Yue, H. Zhang, S. Huang, X.Y. Lin, X. Gao, J. Chang, L.H. Yao, E.J. Guo, Synthesis of ZnO nanowire arrays/3D graphene foam and application for determination of levodopa in the presence of uric acid, Biosens. Bioelectron. 89 (2017) 592–597.
[37] H.Y. Yue, S.S. Song, S. Huang, H. Zhang, X.P.A. Gao, X. Gao, X.Y. Lin, L.H. Yao, E. H. Guan, H.J. Zhang, Preparation of MoS2-graphene hybrid nanosheets and simultaneously electrochemical determination of levodopa and uric acid, Electroanalysis 29 (2017) 2565–2571.
[38] F.R. Figueiredo Leite, C.M. Maroneze, A.B.D. Oliveira, W.T.P.D. Santos, F. S. Damos, R.d.C.S. Luz, Development of a sensor for L-Dopa based on Co(DMG)(2) ClPy/multi-walled carbon nanotubes composite immobilized on basal plane pyrolytic graphite electrode, Bioelectrochemistry 86 (2012) 22–29.
[39] M. Chen, C. Wang, X. Wei, G. Diao, Rapid synthesis of silver nanowires and network structures under cuprous oxide nanospheres and application in surface-enhanced Raman scattering, J. Phys. Chem. C 117 (2013) 13593–13601.
[40] T. Zhang, Y.L. Chen, W. Huang, Y. Wang, X. Hu, A novel AuNPs-doped COFs composite as electrochemical probe for chlorogenic acid detection with enhanced sensitivity and stability, Sensor. Actuator. B Chem. 276 (2018) 362–369.
[41] Y. Liu, Y. Xiang, D. Ding, R. Guo, Structural effects of amphiphilic protein/gold nanoparticle hybrid based nanozyme on peroxidase-like activity and silver-mediated inhibition, RSC Adv. 6 (2016) 112435–112444.
[42] Q.F. Shi, G.W. Diao, S.L. Mu, The electrocatalytic oxidation of glucose on the bimetallic Au-Ag particles-modified reduced graphene oxide electrodes in alkaline solutions, Electrochim. Acta 113 (2014) 335–346.
[43] Z. Wei, W. Wei, L. Yu, W. Fushan, M. Jiantai, Co-Ag alloy protected by nitrogen doped carbon as highly efficient and chemoselective catalysts for the hydrogenation of halogenated nitrobenzenes, J. Colloid Interface Sci. 522 (2018) 217–227.
[44] Y. Xue, Y. Wang, H. Liu, X. Yu, H. Xue, L. Feng, Electrochemical oxygen evolution reaction catalyzed by a novel nickel-cobalt-fluoride catalyst, Chem. Commun. 54 (2018) 6204–6207.
[45] S. Biswas, Y.L. Chen, Y. Xie, X. Sun, Y. Wang, Ultrasmall Au(0) inserted hollow PCN-222 MOF for the high-sensitive detection of estradiol, Anal. Chem. 92 (2020) 4566–4572.
[46] H. Xu, J. Gao, D. Jiang, Stable, crystalline, porous, covalent organic frameworks as a platform for chiral organocatalysts, Nat. Chem. 7 (2015) 905–912.